Shape Factors for the Pseudo-Steady State Flow in Fractured Hydrocarbon Wells of Various Drainage Area Geometries

by

Ankush Sharma

A Thesis Presented in Partial Fulfillment
of the Requirements for the Degree
Master of Science

Approved May 2017 by the
Graduate Supervisory Committee:

Kangping Chen, Co-Chair
Matthew Green, Co-Chair
Heather Emady

ARIZONA STATE UNIVERSITY

August 2017

ABSTRACT

Pseudo-steady state (PSS) flow is an important time-dependent flow regime that quickly follows the initial transient flow regime in the constant-rate production of a closed boundary hydrocarbon reservoir. The characterization of the PSS flow regime is of importance in describing the reservoir pressure distribution as well as the productivity index (PI) of the flow regime. The PI describes the production potential of the well and is often used in fracture optimization and production-rate decline analysis. In 2016, Chen determined the exact analytical solution for PSS flow of a fully penetrated vertically fractured well with finite fracture conductivity for reservoirs of elliptical shape. The present work aimed to expand Chen's exact analytical solution to commonly encountered reservoirs geometries including rectangular, rhomboid, and triangular by introducing respective shape factors generated from extensive computational modeling studies based on an identical drainage area assumption. The aforementioned shape factors were generated and characterized as functions for use in spreadsheet calculations as well as graphical format for simplistic in-field look-up use. Demonstrative use of the shape factors for over 20 additional simulations showed high fidelity of the shape factor to accurately predict (mean average percentage error remained under 1.5 %) the true PSS constant by modulating Chen's solution for elliptical reservoirs. The methodology of the shape factor generation lays the ground work for more extensive and specific shape factors to be generated for cases such as non-concentric wells and other geometries not studied.

DEDICATION

This work is dedicated to my loving parents and sisters who constantly support me in all aspects of my life including my academic endeavors.

ACKNOWLEDGMENTS

Major acknowledgment is given to Dr. Kang Ping Chen for endlessly guiding my research over the past two years and always finding time to aide me in my professional pursuits. Dr. Chen not only made the present work possible but also pushed me farther than I could have gone solely, and aided me in sharing my work.

Further acknowledgment is given to Dr. Matthew Green and Dr. Heather Emady for their attentive support and guidance on the present work and their continued willingness to promptly aide me in completing my research.

TABLE OF CONTENTS

Page

LIST OF TABLES vi

LIST OF FIGURES vii

CHAPTER

1 INTRODUCTION 1

1.1 Background 1

1.2 Pseudo-Steady State 3

1.3 Pseudo-Steady State Characterization 6

1.4 Purpose 9

2 METHODOLOGY 10

2.1 Overview 10

2.2 COMSOL Multiphysics Modeling 10

2.2.1 Rectangular Reservoirs 13

2.2.2 Rhomboid Reservoirs 14

2.2.3 Triangular Reservoirs 15

2.3 Post-Processing 15

3 RESULTS 17

3.1 Rectangular Shape Factor 17

3.2 Rhomboid Shape Factor 19

3.3 Triangular Shape Factor 20

3.4 Demonstrative Use of Shape Factors 23

4 DISCUSSION 26

5 CONCLUSIONS 28

5.1 Future Work 29

CHAPTER Page

REFERENCES 30

APPENDIX

A RECTANGULAR LOOK-UP TABLES 33

B RECTANGULAR SHAPE FACTOR CONFIDENCE INTERVALS 38

C RHOMBOID LOOK-UP TABLE 40

D TRIANGULAR LOOK-UP TABLE 42

E CURVE FITTING STATISTICS 44

LIST OF TABLES

Table Page

1. COMSOL Multiphysics Parameters 12

2. Shape Factor Equations 22

3. Rectangular (Ar = 4) Shape Factor Estimations 23

4. Rhomboid Shape Factor Estimations 24

5. Triangular Shape Factor Estimations 24

6. Rectangular (AR = 1) Shape Factor Look-Up Table 34

7. Rectangular (AR = 2) Shape Factor Look-Up Table 35

8. Rectangular (AR = 3) Shape Factor Look-Up Table 36

9. Rectangular (AR = 4) Shape Factor Look-Up Table 37

10. Rhomboid Shape Factor Look-Up Table 41

11. Triangular Shape Factor Look-Up Table 43

12. Shape Factor Curve Fitting Statistics 45

LIST OF FIGURES

Figure Page

1. Illustration of a Fully Penetrated Vertically Fractured Well in a Bounded Reservoir (Lei 2012) 2
2. Illustration of Stresses and Fracture Interplay in Rock Formations (Valko 2005) 3
3. Pressure Distribution Visualized along the Radial Coordinate of a Constantly Producing Well 4
4. Elliptical Reservoir Geometry with a Fully Penetrated Fracture Modelled by a Long Thin Ellipse. The Illustration Does Not Reflect Actual Scales. 7
5. The Dimensionless Pressure Drawdown at the Well Plotted as a Function of Dimensionless Time Based on Drainage Area. The PSS Constant Is Found at the Ordinate Intercept of a Tangent Line that Is Drawn to the Curve When the Slope Is 2π. 11
6. Planar View of a Rectangular Closed Reservoir with Centrally Located Fully Penetrated Vertically Fractured Well. The Illustration Does Not Reflect Actual Scales. 13
7. Planar View of a Rhomboid Closed Reservoir with Centrally Located Fully Penetrated Vertically Fractured Well. The Illustration Does Not Reflect Actual Scales. 14
8. Planar View of a Triangular Closed Reservoir with Centrally Located Fully Penetrated Vertically Fractured Well. The Illustration Does Not Reflect Actual Scales. 15

Figure Page

9. Dimensionless Wellbore Pressure Drawdown Plotted as a Function of Drainage Area Based Dimensionless Time for a Rectangular (AR = 2) Reservoir Geometry Simulation 17

10. Rectangular Shape Factor for Various Penetration and Aspect Ratios 18

11. Dimensionless Wellbore Pressure Drawdown Plotted as a Function of Drainage Area Based Dimensionless Time for a Rhomboid Reservoir Geometry Simulation 19

12. Rhomboid Shape Factor for Various Penetration Ratios 20

13. Dimensionless Wellbore Pressure Drawdown Plotted as a Function of Drainage Area Based Dimensionless Time for a Triangular Reservoir Geometry Simulation 21

14. Rhomboid Shape Factor for Various Penetration Ratios 22

15. 95 % Confidence Intervals for Rectangular Shape Factors 39

Chapter 1

INTRODUCTION

1.1 Background

In the context of petroleum engineering, hydrocarbons that have been stored subsurface in permeable rock formations are termed reservoirs. A well (vertical or horizontal) is then drilled into the reservoir to extract the hydrocarbons in place for downstream processing and later, commercial use. The features and relative geometries of a hydrocarbon reservoir and associated well often dictate many of the production aspects the well will produce in its lifetime (Chen 2016).

A simplified two-dimensional analog of a reservoir shape is often used to describe the reservoir geometry or commonly referred to as a drainage area. The most commonly seen shapes include circles, squares, parallelograms, and triangles among others (Hagoort 2011; Sadeghi, Shadizadeh, and Ahmadi 2013; Dietz 1965). Moreover, sealing faults such as less permeable rocks as well as nearby equally spaced wells producing at similar rates can cause a reservoir to have closed boundaries that consequentially make an impermeable barrier and thus a finite drainage area (Beaumont Norman H. 1999) (Figure 1).

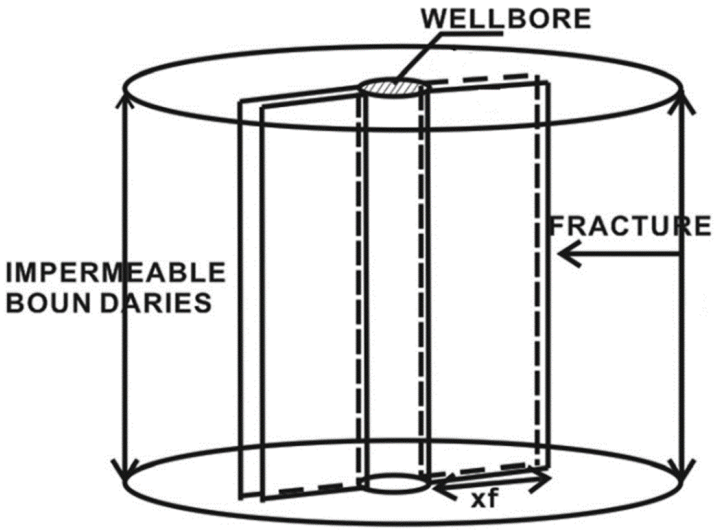

Figure 1. Illustration of a fully penetrated vertically fractured well in a bounded reservoir (Lei 2012)

The rock formation in a reservoir is often fractured to enhance production at the well. Fractures are generally horizontal or vertical and their propagation depends on the minimal principal stress vector. More specifically, fractures tend to propagate perpendicular to the applied minimal principal stress on the rock (Hubbert and Willis 1957) (Figure 2). Further, a fracture is fully penetrated when it runs the distance of producing well section. In this enhanced production, two driving mechanisms compete to produce reservoir fluid; the low pressure inside the wellbore drawing fluid towards its region ; and the highest pressure gradient near the fracture tip in the reservoir (Chen, Jin, and Chen 2013). The fluid flow through the fracture most often dominates as it provides a path of least resistance towards the wellbore (i.e. a fracture permeability can be several orders of magnitude larger than the reservoir's) (Chen, Jin, and Chen 2013; Jin, Chen, and Chen 2015a, 2015b). Chen et al. also found that the production was strongly dependent on the fracture penetration ratio which was defined as the ratio of the fracture half-length and characteristic reservoir extent.

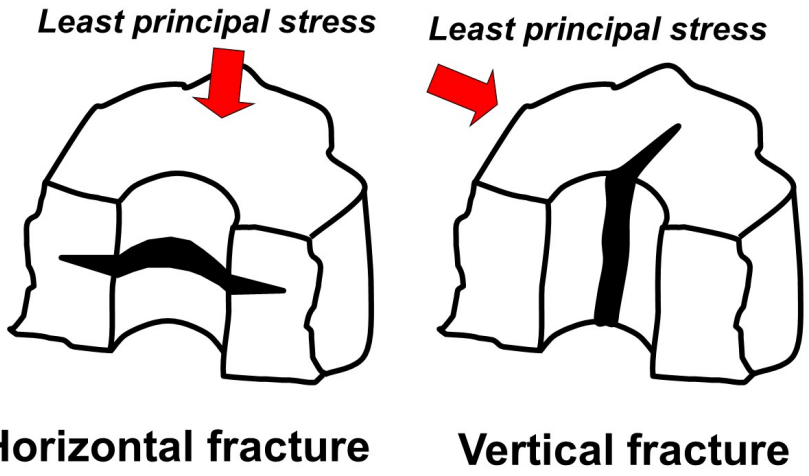

Figure 2. Illustration of stresses and fracture interplay in rock formations (Valko 2005)

1.2 Pseudo-Steady State

The constant rate production of a closed reservoir generally occurs in three distinct time-phases that describe the pressure drawdown in the drainage area. Moving from start to completion, these time-phases include the early-, middle-, and late-time regions.

During the early-time region, the effects of the wellbore and wellbore-area are felt such as wellbore storage and phase redistribution (Figure 3). As production moves to the middle-time region, the transient flow is driven by outward diffusion of the pressure drawdown. In the late-time region, the diffusion of the pressure drawdown reaches the closed boundary and a pseudo-steady state (PSS) flow begins as boundary effects begin to be felt. During this regime the PSS flow is driven by the volumetric

compression of the reservoir and a constant rate of pressure decline is felt at all points within the reservoir drainage area (Ramey and Cobb 1971).

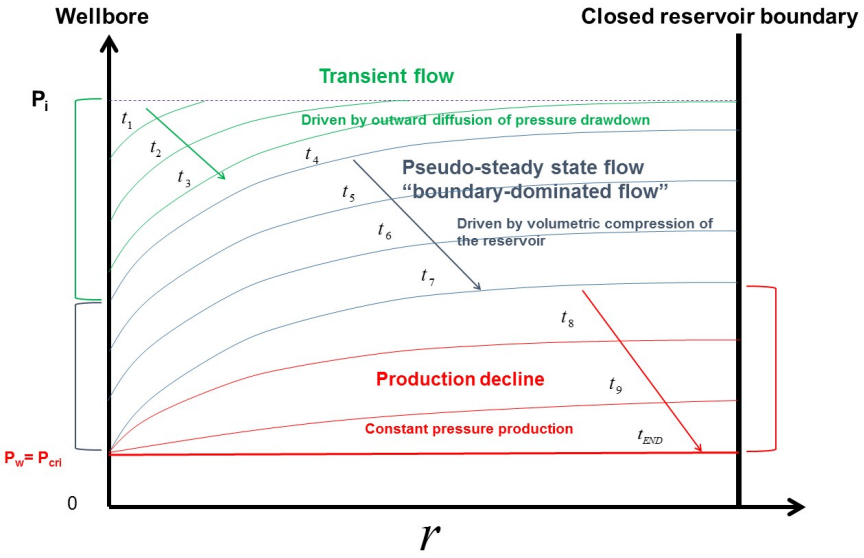

Figure 3. Pressure distribution visualized along the radial coordinate of a constantly producing well

The PSS flow regime in the late-time region of a constantly producing well can be quite lengthy depending on the reservoir configuration and geometry. In this time frame, the reservoir pressure is set by the production rate and drainage area and decreases linearly with time. The so-called "PSS solution" is often used to mathematically describe the reservoir pressure field in the late-time region (Hagoort 2011).

The constant rate production during the PSS flow regime comes to a hault when the bottomhole well pressure reaches a critical mimumum, such that the production declines with time during a constant pressure production. Production rate decline analysis is a large area of study during this flow period and is often used to determine the economically feasible amount of hydrocarbons that can be recovered from the

reservoir (Arps 1945; Fetkovich et al. 1987; Economides et al. 2013). The PSS solution is included in various production analyses during this period as it immediately proceeds the production rate decline period (Doublet and Blasingame 1995; Fetkovich 1980). More specifically, the dimensionless PSS pressure drawdown at the wellbore is used in these analyses and is described as

$$\Delta p_{wD,PSS} = 2\pi t_{DA} + b_{D,PSS} \tag{1.1}$$

where t_{DA} is the dimensionless time based on drainage area, and $b_{D,PSS}$ is the commonly termed PSS constant. The characteristic drainage-area based time and characteristic pressure drawdown at the wellbore are nondimensionalized to form these variables as such,

$$t_{DA} = \frac{\kappa t}{\mu c_t \phi A} \tag{1.2}$$

and

$$\Delta p_{wD,PSS} = \frac{2\pi\kappa h}{\mu Q_D}\left(p_{i,d} - p_{w,d}\right) \tag{1.3}$$

where κ is the permeability of the reservoir, h is the formation thickness, μ is the fluid viscosity, Q_D is the volumetric production rate of the well, ϕ is the reservoir porosity, c_t is the total compressibility of the reservoir,$p_{i,d}$ is the initial fluid pressure in the reservoir, A is the drainage area, and $p_{w,d}$ is the pressure drawdown at the well.

The PSS constant is integral to the PSS solution description as it is used to scale the dimensionless time and rate of pressure decline within the reservoir and is dependent on the parameters such as the relative wellbore location, reservoir geometry, fracture orientation and penetration ratio (Chen 2016). Further, the PSS constant is

directly related to the productivity index (PI) of a well and therefore directly related to the dimensionless PI, $J_{D,PSS}$ by

$$J_{D,PSS} \equiv \frac{1}{b_{D,PSS}}. \tag{1.4}$$

The PI is an extremely important parameter that describes the fluid production per unit pressure drop of a well and has been shown to play a role in fracture optimization and production optimization (Jin, Chen, and Chen 2015a, 2015b; Lu and Chen 2016). For these reasons, the PSS constant is an extremely important characteristic to determine for a producing well.

1.3 Pseudo-Steady State Characterization

For unfractured wells in common reservoir geometries, analytical solutions to the PSS constant are well defined (Hagoort 2011; Raghavan 1993) and can be generalized for more geometries with shape factors such as those generated by Dietz (Dietz 1965).

Historically, an exact analytical solution for the PSS flow in a circular fractured reservoir approximated with an elliptical shape was mathematically derived by Prats et al. in 1962 (Prats, Hazebroek, and Strickler 1962). More specifically the solution was obtained for a vertically fractured well with closed boundaries. Prats solution was however based on an unrealistic assumption of infinite fracture conductivity, hindering it's applicability and accuracy (Chen 2016). In 2016, Chen was able to extend the work of Prats and determine the exact analytical solution to describe the PSS flow (and therefore the PSS constant) in a fully penetrated vertically fractured well with finite conductivity and large elliptical shape similar to Figure 4 (ibid).

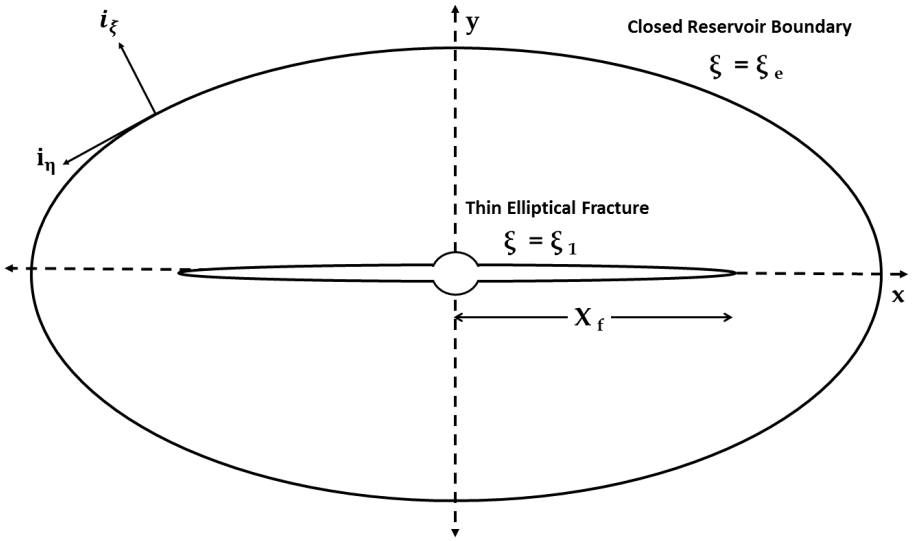

Figure 4. Elliptical reservoir geometry with a fully penetrated fracture modelled by a long thin ellipse. The illustration does not reflect actual scales.

Where X_f is the fracture half-length and the closed elliptical reservoir shape, ξ_e is described in elliptical coordinates by ξ and η such that the coordinates can be derived from their Cartesian counterparts by

$$x = X_f cosh(\xi) cos(\eta) \tag{1.5}$$

$$y = X_f sinh(\xi) sin(\eta) \tag{1.6}$$

Further, the fully penetrated vertical fracture shape is described by an ellipsoid ξ_1, such that the fracture half-length X_f is much larger than the fracture width. For this case, Chen's solution for the PSS constant was found to be

$$b_{D,PSS} = \xi_e + \frac{1}{sinh(2\xi_e)} - \frac{3}{4} coth(2\xi_e) + \frac{2a_1}{sinh(2\xi_e)} + \frac{1}{F_E}\left(\frac{\pi^2}{6} + 4a_1 - \sum_{n=2}^{\infty} \frac{1}{n^2} \frac{1}{1 + nF_E coth(2n\xi_e)}\right) \tag{1.7}$$

with

$$a_1 = -\frac{1}{8}\frac{1}{cosh(2\xi_e) + \frac{sinh(2\xi_e)}{F_E}}\left(1 + \frac{2}{F_E}sinh(2\xi_e)\right). \tag{1.8}$$

Where, F_E is the dimensionless elliptical fracture conductivity described by

$$F_E = \frac{\kappa_f w_f}{\kappa X_f} \tag{1.9}$$

and κ_f is the permeability of the fracture, and w_f represents the fracture width. The solution has also been shown to accurately model circular drainage areas with a shape-approximation-induced error of less than 1 % for fracture penetration ratios up to 53 % (Lu and Chen 2016).

Despite this promising new analytical solution for elliptical wells, there are still gaps in determining an accurate solution for the PSS constant for geometries outside of elliptical or circular. Several groups have produced approximate solutions for reservoir geometries including square and rectangular (Lu and Tiab 2010; Goode and Kuchuk 1991; Hagoort 2009; Russell and Truitt 1964; Matthews, Brons, and Hazebroek 1954), however many of the approximations contained flawed assumptions and bases. The alternative to determine an accurate PSS constant is through the numerical simulation of each reservoir of interest, which has been documented as extremely time consuming and mathematically intensive as the PSS constant can be subtracted from the scaled drainage area based dimensionless time when the long-time data set of dimensionless pressure drawdown is found (Blasingame, Amini, and Rushing 2007).

1.4 Purpose

The purpose of this research is to determine and execute a suitable general methodology to generate high fidelity shape factors to modify Chen's PSS constant solution for fully penetrated vertically fractured wells in a closed elliptical reservoir. More specifically shape factors to modify the exact PSS solution for rectangular, triangular, and rhomboid closed reservoir geometries with concentric fully penetrated vertically fractured wells are considered.

Chapter 2

METHODOLOGY

2.1 Overview

The general procedure to create shape factors that augment Chen's solution was to determine the true PSS constant for various reservoir geometries and then compare it to a PSS constant approximation from the elliptical reservoir analytical solution based on an assumed equivalence point. Then, by ratioing the true and predicted solution over several case studies of a geometry, trends could be observed and characterized in order to create a shape factor that modulates Chen's solution accordingly to accurately describe the true PSS constant.

2.2 COMSOL Multiphysics Modeling

Consider a fully penetrated vertically fractured well centrally located in a closed reservoir of generic shape. The well is producing at a constant rate and a sufficient period of time has passed such that outer-boundary effects are being felt and the fluid is described by PSS flow. The flowing reservoir fluid is assumed to be single-phase in a homogeneous formation, where the fluid and reservoir are weakly compressible and can thus be described by a single lumped compressibility constant. The fracture is assumed to be supported by proppants and is considered incompressible. Moreover, the permeability of the fracture is taken to be much larger than the formation inferring that all production is from the fracture. The fracture is width is also defined to be

much smaller than the length of the fracture as well as the diameter of the wellbore. The fluid motion in the finite formation and fracture is governed by Darcy's law, and any effects of wellbore storage and skin are negligible.

Further, consider the dimensionless pressure drawdown at the well plotted as a function of the dimensionless time based on drainage area (Figure 5). As the producing well begins to feel the effects of the no-flow boundaries in the late-time region, the pressure drawdown within the reservoir becomes constant. The true PSS constant can directly be determined at the ordinate intersection of a tangent line that shares a slope of 2π with the curve.

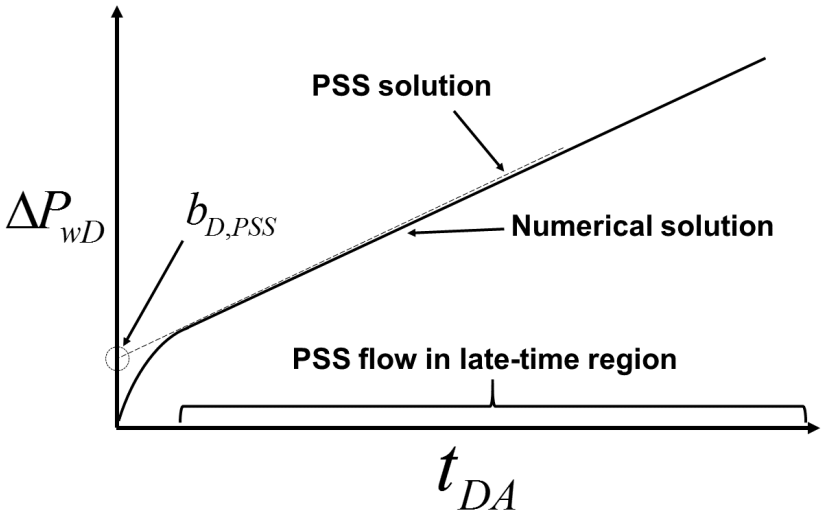

Figure 5. The dimensionless pressure drawdown at the well plotted as a function of dimensionless time based on drainage area. The PSS constant is found at the ordinate intercept of a tangent line that is drawn to the curve when the slope is 2π.

If a similar well is considered with an equal drainage area but with an elliptical reservoir geometry, an approximation can be made by Chen's formulation for the PSS constant for the similar case. Thus a shape factor can be defined as

$$C_{a,f} \equiv \frac{b_{D,PSS}}{b_{D,PSSA}} \tag{2.1}$$

where $b_{D,PSS}$ is the true PSS constant of the case study and $b_{D,PSSA}$ is the approximated PSS constant using the exact analytical solution for reservoirs of elliptical shape. Thus a shape factor for a particular well geometry and configuration is made which corrects the approximation to the true value. If several case studies with variable penetration ratios are completed for a certain geometry, the shape factor can be applied to a larger set of reservoir configurations through interpolations and curve fitting.

Table 1. COMSOL Multiphysics Parameters

Parameter	Value	Description
c_f	1E-11$[Pa^{-1}]$	Formation compressibility
c_l	1E-10$[Pa^{-1}]$	Fluid compressibility
ρ_o	1E6$[kg/m^3]$	Initial fluid density
ϕ_o	5E-2[-]	Initial formation porosity
κ	1$[mD]$	Formation permeability
μ	1E-3$[Pa \cdot s]$	Fluid viscosity

COMSOL Multiphysics was used to simulate the transient pressure field of a reservoir for a series of penetration ratios in reservoir geometries of rectangular, triangular, and rhomboid shape. Table 1 shows various parameters used in the configuration of each simulation. All cases were modelled as a two dimensional radial slice of the reservoir as solution symmetry is seen in the axial direction of the well. Darcy's law modules were used to manage the fluid flow field in the fracture and reservoir, and fractured flow conditions in the Subsurface Module were used to build out and maintain fractures in the geometry. Further, no-flow boundary conditions

were made at the reservoir boundaries to simulate a closed finite formation. The well was located centrally across all case studies in the present work for simplicity. Along with the aforementioned assumptions, the following parameters were also used in all case studies to define the well configuration and case study. The penetration ratio for each case study was varied by maintaining a constant characteristic boundary length while modulating the fracture half-length.

2.2.1 Rectangular Reservoirs

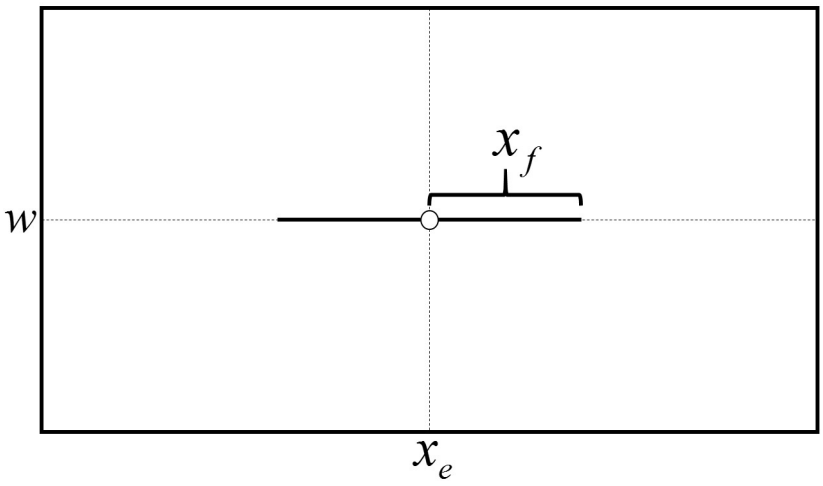

Figure 6. Planar view of a rectangular closed reservoir with centrally located fully penetrated vertically fractured well. The illustration does not reflect actual scales.

A rectangular reservoir with centrally located well (Figure 6) was defined to have an aspect ratio, AR such that

$$AR \equiv \frac{x_e}{w} \tag{2.2}$$

where x_e was the reservoir characteristic side length (reservoir drainage extent) and w was the reservoir width. The rectangular penetration ratio was defined as

$$I_x = \frac{2x_f}{x_e} \tag{2.3}$$

where x_f was the fracture half-length. Rectangular geometries of aspect ratio 1 (square), 2, 3, and 4 were studied at various penetration ratios up to 50% as ratios above this are rarely seen in-field.

2.2.2 Rhomboid Reservoirs

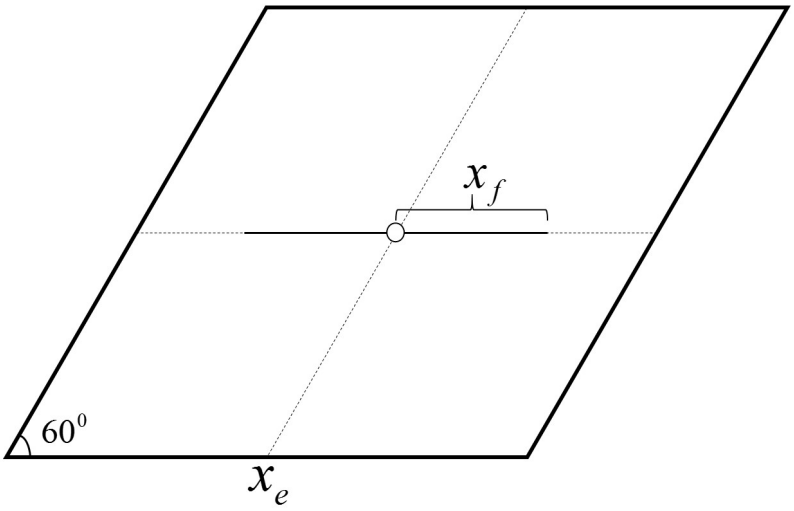

Figure 7. Planar view of a rhomboid closed reservoir with centrally located fully penetrated vertically fractured well. The illustration does not reflect actual scales.

Rhomboid geometries were studied in suit with the rectangular geometries (Figure 7). The penetration ratio was defined similarly to the rectangular case. Note, the acute angle of the reservoir shape was 60 °.

2.2.3 Triangular Reservoirs

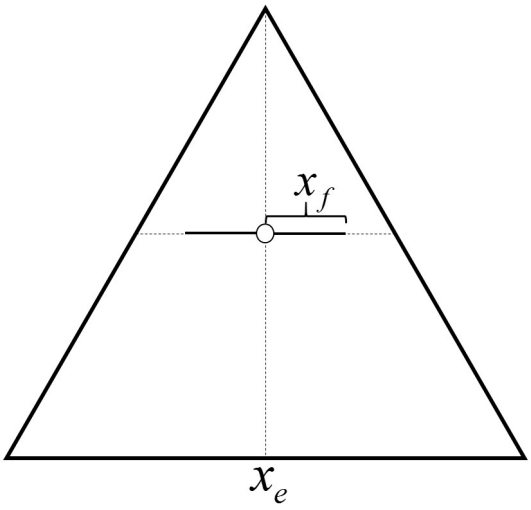

Figure 8. Planar view of a triangular closed reservoir with centrally located fully penetrated vertically fractured well. The illustration does not reflect actual scales.

Equilateral triangle shaped reservoirs with centrally located wells (Figure 8) were studied at various penetration ratios up to 50% . The penetration ratio for the equilateral triangle was defined slightly differently as,

$$I_x = \frac{4x_f}{x_e} \tag{2.4}$$

2.3 Post-Processing

From the COMSOL Multiphysics simulations, MATLAB was used for post-processing of the transient pressure field data. More specifically, the transient pressure field data at the wellbore in the mesh was used to calculate the time dependent wellbore pressure drawdown as described by Equation 1.3.The dimensionless drainage

area based time was calculated by Equation 1.2. The true PSS constant could then be determined as previously described and compared to an approximation of the PSS constant by Chen's solution assuming an equal drainage area.

Once the shape factors were determined, two parameter one-variable curve fitting via non-linear regression was conducted by fitting curve shapes to over 200 non-linear functions in Lab Fit to determine the form with the least residual error and root mean squared error.

Chapter 3

RESULTS

3.1 Rectangular Shape Factor

The relationship between Δp_{wD} and t_{DA} was first plotted to ensure the dimensionless drawdown pressure reached a constant sloping trend (Figure 9), indicating production in the late-time region under a PSS flow regime. The "PSS Solution" called out associates with Equation 1.1 and the "Numerical Solution" called out refers to results obtained from the reservoir simulation.

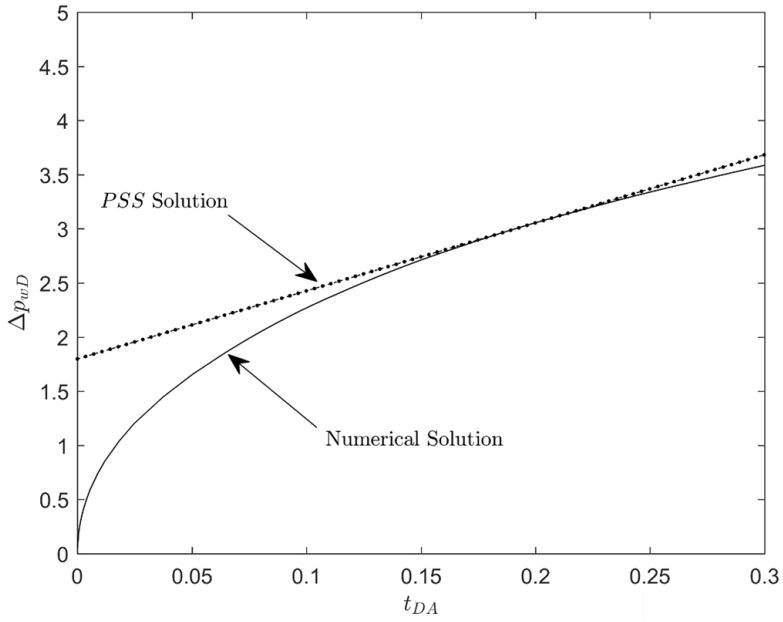

Figure 9. Dimensionless wellbore pressure drawdown plotted as a function of drainage area based dimensionless time for a rectangular (AR = 2) reservoir geometry simulation

By ratioing the true and approximated solutions of the PSS constant, the shape

factor for a rectangular well was made for geometry's with various aspect ratios and fracture penetration ratios. Figure 10, shows the rectangular shape factor curves for reservoir geometries that have an aspect ratio between one and four for penetration ratios less than 50 %. For each geometry, approximately 20 case studies were numerically studied with variable penetration ratios linearly spaced between up to 50 %.

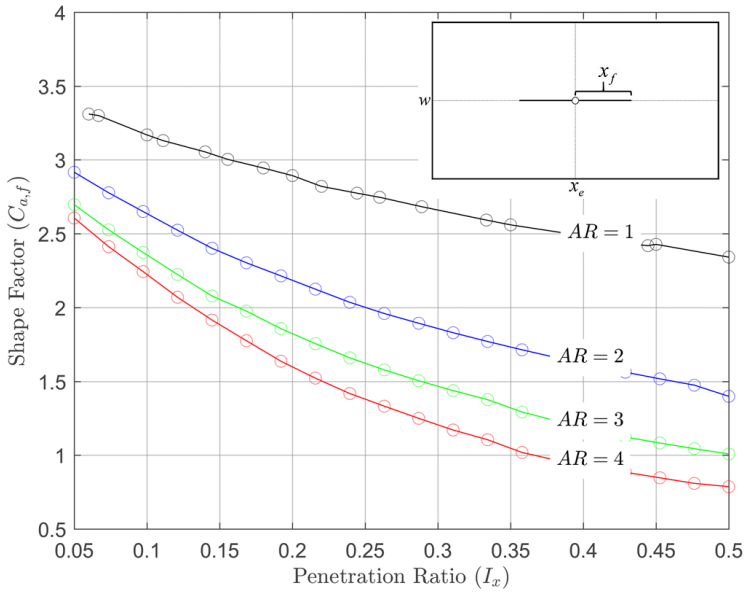

Figure 10. Rectangular shape factor for various penetration and aspect ratios

From the plot it can be seen that as the penetration ratio increases the shape factor decreases in a non-linear fashion. Through trial and error, all curves were fitted to high degrees of accuracy with either an inverse linear or modified logarithmic trend. These equations can be seen in Table 2 below and represent the lines through Figure 10. Additionally, a look-up table format of similar data is presented in Appendix A for the rectangular shape factors. Further, 95 % confidence intervals for each curve fit can be found in Appendix B.

3.2 Rhomboid Shape Factor

Similar to the rectangular shape factor results, dimensionless pressure drawdown at the well was plotted as a function of the dimensionless drainage area based time for every case to determine if the simulation had reached the late-time region in which PSS flow occurs. Figure 11 displays one of the plots generated to determine if PSS flow actually occurred.

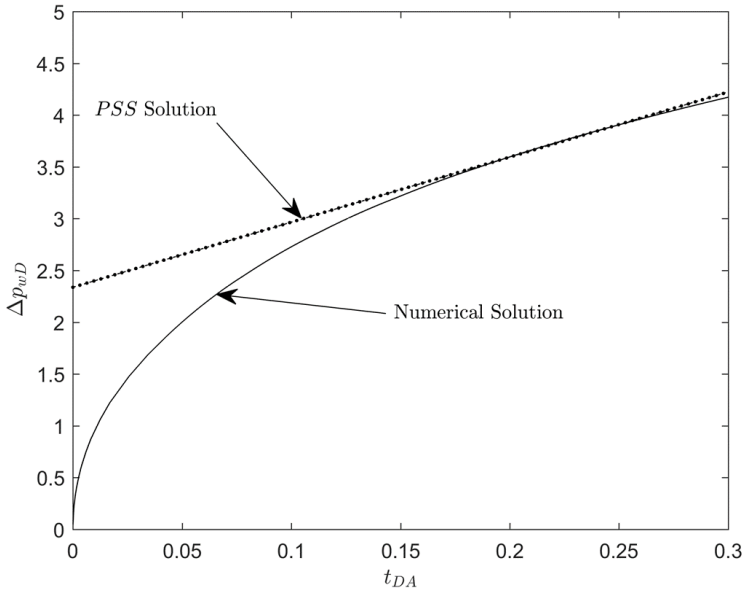

Figure 11. Dimensionless wellbore pressure drawdown plotted as a function of drainage area based dimensionless time for a rhomboid reservoir geometry simulation

From the plot it is clear that the simulation reached PSS flow as it asymptotically approached and followed the PSS Solution trend. Once the PSS flow regime was confirmed for all case studies, approximate and numerically simulated PSS constants were derived and partitioned to create shape factors based on penetration ratios (Figure 12). Additionally, a look-up table format of similar data is presented in Appendix C for the rhomboid shape factor.

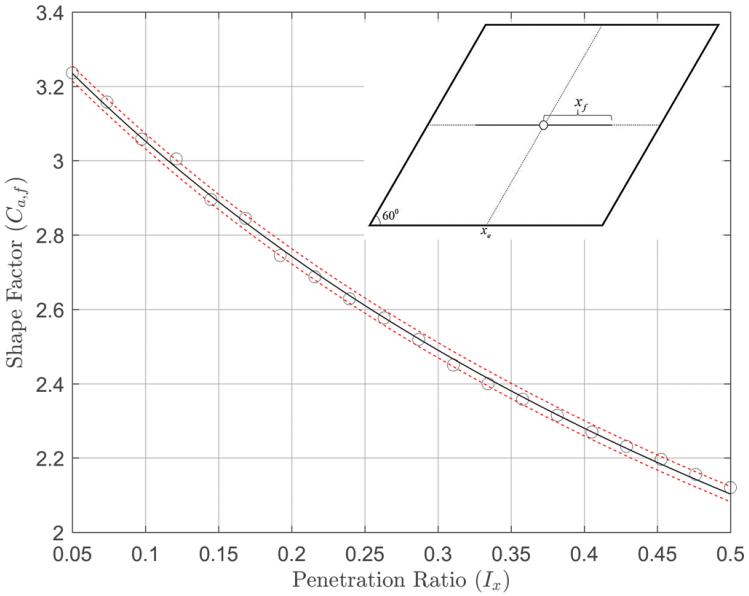

Figure 12. Rhomboid shape factor for various penetration Ratios

Within Figure 12, the data points are indicated by circles while a curve fitted trend line and associated 95 % confidence intervals are displayed as a solid black line and red dotted line respectively. Similar to the rectangular shape factors, as the penetration ratio increased to 50 %, the shape factor decreased. Additionally, the curve fit equation was of inverse linear form and can be viewed in Table 2 while associated statistics are detailed in Appendix E.

3.3 Triangular Shape Factor

Figure 13 shows a plot of Δp_{wD} as a function of t_{DA} for a simulation with a triangular reservoir geometry.

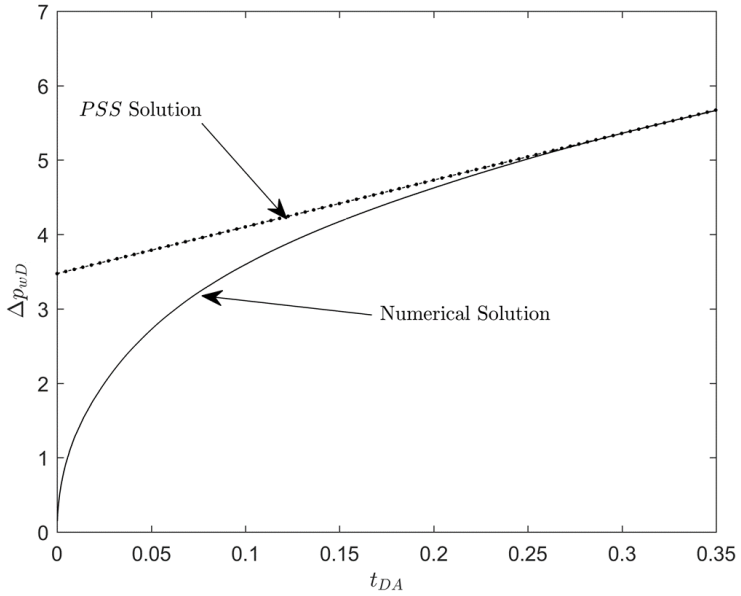

Figure 13. Dimensionless wellbore pressure drawdown plotted as a function of drainage area based dimensionless time for a triangular reservoir geometry simulation

The numerical simulation is seen approaching the PSS solution indicating the flow regime did indeed reach PSS flow. Figure 14 below shows the triangular shape factor plotted as a function of penetration ratio.

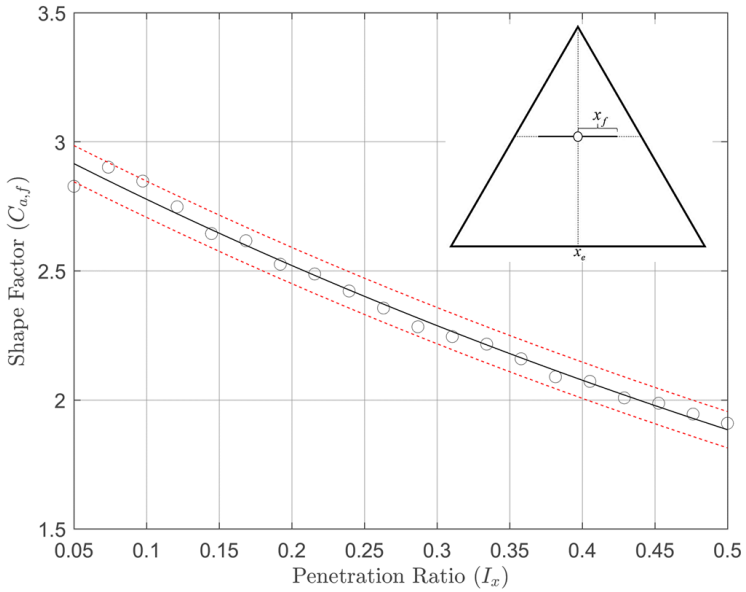

Figure 14. Rhomboid shape factor for various penetration Ratios

Similar to the rhomboid shape factor, the black solid line represents the curve fitted equation (modified exponential form) while the dashed red lines represent the 95 % confidence interval. Additionally, a look-up table format of similar data is presented in Appendix D for the triangle shape factor. The curve fitted equation is found in Table 2 while associated statistics are found in Appendix E for all curve fit equations.

Table 2. Shape Factor Equations

Shape	A	B	$C_{a,f}$ Form
Rectangle (AR 1)	0.2931	0.2863	$(AI_x + B)^{-1}$
Rectangle (AR 2)	0.7914	0.3015	$(AI_x + B)^{-1}$
Rectangle (AR 3)	1.3130	0.2965	$(AI_x + B)^{-1}$
Rectangle (AR 4)	-1.205	0.0618	$Aln(I_x + B)$
Rhomboid	0.3698	0.2906	$(AI_x + B)^{-1}$
Equilateral Triangle	3.060	-0.970	$Aexp(BI_x)$

3.4 Demonstrative Use of Shape Factors

Rearranging Equation 2.1, the true $b_{D,PSS}$ is expressed in terms of Chen's approximation of the PSS constant relabelled as $b_{D,PSSA}$ and the shape factor $C_{a,f}$.

$$b_{D,PSS} = C_{a,f} b_{D,PSSA} \tag{3.1}$$

The shape factor is conveniently only a function of the reservoir's penetration ratio, while the approximation is in terms of commonly known reservoir properties. Thus, Equation 3.1 is a quick method to determine a $b_{D,PSS}$ value that truly represents the reservoir of interest. To demonstrate the usage and fidelity of the shape factor, over 15 reservoir simulations were made to determine the accuracy at which the shape factor modification to Chen's solution could predict $b_{D,PSS}$ values that were not used in its generation.

Five simulations were done at various penetration ratios of a rectangular well with an aspect ratio of four (Table 3.

Table 3. Rectangular (Ar = 4) Shape Factor Estimations

I_x	$C_{a,f}$	Init. $b_{D,PSSA}$	Final $b_{D,PSSA}$	True $b_{D,PSS}$	Error (%)
0.09	2.24	2.43	5.45	5.50	0.76
0.19	1.68	1.76	2.96	2.93	1.13
0.26	1.35	1.42	1.92	1.89	1.68
0.35	1.08	1.17	1.25	1.22	2.97
0.40	0.93	1.04	0.96	0.97	0.54

The known penetration ratio was used to calculate the necessary shape correction factor, which was then multiplied by the initial calculated $b_{D,PSSA}$ from the approximating solution. This value was then compared to the true $b_{D,PSS}$ of the

simulated reservoir and an absolute error in percent was calculated. From Table 3, the approximations from the modified Chen solution were highly accurate, with the highest approximation error being approximately three percent. Five simulations with rhomboid reservoir shapes were also tested to gauge the ability of the rhomboid shape factor (Table 4).

Table 4. Rhomboid Shape Factor Estimations

I_x	$C_{a,f}$	Init. $b_{D,PSSA}$	Final $b_{D,PSSA}$	True $b_{D,PSS}$	Error (%)
0.06	3.20	2.88	9.21	9.31	1.02
0.16	2.87	1.93	5.55	5.60	0.86
0.20	2.74	1.69	4.63	4.61	0.48
0.34	2.40	1.19	2.85	2.85	0.06
0.42	2.24	1.00	2.24	2.26	0.81

Table 4 shows that the rhomboid shape factor retains high fidelity over the tested simulations as the absolute errors were no larger than approximately one percent. Lastly, seven simulations with triangular reservoir geometries and various penetration ratios were studied to test the triangle shape factor (Table 5).

Table 5. Triangular Shape Factor Estimations

I_x	$C_{a,f}$	Init. $b_{D,PSSA}$	Final $b_{D,PSSA}$	True $b_{D,PSS}$	Error (%)
0.10	2.78	3.06	8.51	8.70	2.16
0.26	2.37	2.10	4.97	4.94	0.62
0.36	2.16	1.79	3.87	3.86	0.15
0.39	2.10	1.72	3.61	3.62	0.12
0.48	1.92	1.51	2.91	2.96	1.78
0.52	1.84	1.43	2.63	2.67	1.29
0.57	1.76	1.35	2.37	2.46	3.55

Table 5 shows that the triangle shape factor retains high accuracy for the simu-

lations studied. It is worthy to note that two scenarios were tested over the 50 % penetration ratio cap, and high accuracy was still achieved, as the error remained under five percent.

Chapter 4

DISCUSSION

Shape factors for concentrically placed wells in rectangular, rhomboid, and triangular reservoir geometries were successfully derived for penetration ratios below 50 % which are ratios most commonly seen in-field. Further, all shape factor curves were characterized using non-linear regression. All regression models were in terms of inverse linear, modified exponential, or modified logarithm functions with $I_{[}x]$ as a sole variable and two regression coefficients. The culminating results of the work were presented in Figures 10,12, and 14 which graphically displayed the various shape factors and Table 2 which compiled all the curve fitted equations that characterize the generated shape factor curves.

Nearly 80 various well configurations were simulated in rectangular reservoirs to generate shape factors for rectangular reservoir drainage areas with aspect ratios ranging between one and four. Further, 20 various well configurations were simulated for both rhomboid and triangular reservoir shapes to generate shape factors. Due to all the shape factor data generally following smooth trends, curve fitting was found to be quite successful at describing the data sets. This was visualized with tight 95% confidence intervals and backed by further statistics seen in Appendix E. For example, the mean absolute percentage error for out of sample validation was found to be 1.41 % , 1.38 %, and 0.65 % for the rectangular, triangular, and rhomboid shape factors respectfully. Further the root mean squared error for all curve fits were under 0.02, indicating that the regressor coefficients and accompanying form for each fit was predicting data with high accuracy.

For the rectangular shape factors, as the aspect ratio increased, the shape factor curve translated lower. A lower shape factor indicates that the unmodified approximation was closer to the true PSS value when compared to higher shape factor numbers. In speculation, reservoirs with larger aspect ratios may be more geometrically similar to the ellipsoid, ξ_e that is approximating it when compared to reservoirs with smaller aspect ratios. Additionally, for all shape factors, as the I_x increased to 50 % the shape factor decreased in a non-linear fashion. In conjecture, this could be because the large penetration ratios indicate larger fractures which may be more geometrically similar to the penetration ratio definition for elliptical wells.

Chapter 5

CONCLUSIONS

The PSS constant is an important parameter that is used to describe the PSS dimensionless pressure drawdown at the well in a reservoir during the late-time region of fluid production. The PSS also directly relates to the dimensionless PI of a well which has been shown to be important during fracture optimization and production rate decline analysis.

In 2016, Chen mathematically derived the exact analytical solution to describe the PSS constant in a fully penetrated vertically fractured well in an elliptical reservoir. By using extensive computational modeling, the current work extends Chen's solution by introducing shape factors to widen the applicability to wells of rectangular, rhomboid, and triangular reservoir geometries. More specifically, shape factors were made for concentric wells in rectangular geometries of AR 1-4, equilateral triangles, and rhomboids. The shape factors were made a function of the penetration ratio and are applicable under $I_x \leqslant 50\%$. Further, characterization using curve fitting was conducted for quick spreadsheet calculations while look-up tables were generated for in-field use. Example usage of the shape factors was conducted and demonstrated the high fidelity of the shape factors to reproduce accurate PSS constant predictions. Across all shape factors, the mean absolute error in validation case studies were under 1.5 % using the curve fitted equations that were generated in Table 2.

5.1 Future Work

This work has laid the foundation methodology to create additional shape factors to describe various well configurations not studied presently. In the immediate future, shape factors for parallelograms with various aspect ratios and reservoirs with non-concentric wells should be studied to build out the coverage of shape factors to modulate Chen's solution. Lastly, the effects of fracture orientation within these geometries would provide a more complete package for the shape factors to be used.

REFERENCES

Arps, J.J. 1945. "Analysis of Decline Curves." *Transactions of the AIME* 160, no. 01 (): 228–247. doi:10.2118/945228-G.

Beaumont Norman H., Edward A Foster, ed. 1999. *Exploring for Oil and Gas Traps.* American Association of Petroleum Geologists. http://geoscienceworld.org/content/9781629810744/9781629810744.

Blasingame, Thomas Alwin, Shahram Amini, and Jay Rushing. 2007. "Evaluation of the Elliptical Flow Period for Hydraulically-Fractured Wells in Tight Gas Sands – Theoretical Aspects and Practical Considerations." In *SPE Hydraulic Fracturing Technology Conference.* College Station, Texas, U.S.A: Society of Petroleum Engineers. doi:10.2118/106308-MS.

Chen, Kang Ping. 2016. "Production From a Fractured Well With Finite Fracture Conductivity in a Closed Reservoir: An Exact Analytical Solution for Pseudosteady-State Flow." *SPE Journal* 21, no. 02 (): 550–556. doi:10.2118/179739-PA.

Chen, Kang Ping, Yan Jin, and Mian Chen. 2013. "Pressure-gradient singularity and production enhancement for hydraulically fractured wells." *Geophysical Journal International* 195, no. 2 (): 923–931. doi:10.1093/gji/ggt272.

Dietz, D.N. 1965. "Determination of Average Reservoir Pressure From Build-Up Surveys." *Journal of Petroleum Technology* 17, no. 08 (): 955–959. doi:10.2118/1156-PA.

Doublet, L.E., and T.A. Blasingame. 1995. "Decline Curve Analysis Using Type Curves: Water Influx/Waterflood Cases." In *1995 Annual SPE Technical Conference and Exhibition.* Dallas, TX, USA: Society of Petroleum Engineers.

Economides, Michael J., Daniel A. Hill, Christine Ehlig-Economides, and Ding Zhu. 2013. *Petroleum production systems.* 2nd ed. Upper Saddle River: Prentice Hall.

Fetkovich, M J, M E Vienot, M D Bradley, and U G Kiesow. 1987. "Decline Curve Analysis Using Type Curves: Case Histories." *SPE Formation Evaluation* 2 (4): 637–656. doi:10.2118/13169-PA.

Fetkovich, M.J. 1980. "Decline Curve Analysis Using Type Curves." *Journal of Petroleum Technology* 32, no. 06 (): 1065–1077. doi:10.2118/4629-PA.

Goode, P.A., and F.J. Kuchuk. 1991. "Inflow Performance of Horizontal Wells." *SPE Reservoir Engineering* 6, no. 03 (): 319–323. doi:10.2118/21460-PA.

Hagoort, Jacques. 2009. "The Productivity of a Well with a Vertical Infinite-Conductivity Fracture in a Rectangular Closed Reservoir." *SPE Journal* 14, no. 04 (): 715–720. doi:10.2118/112975-PA.

———. 2011. "Semisteady-State Productivity of a Well in a Rectangular Reservoir Producing at Constant Rate or Constant Pressure." *SPE Reservoir Evaluation & Engineering* 14, no. 06 (): 677–686. doi:10.2118/149807-PA.

Hubbert, M K, and D G Willis. 1957. "Mechanics of Hydraulic Fracturing." *Transactions of the AIME* (420 Commonwealth Dr, Warrendale, PA 15086) 210 (6): 153–163.

Jin, Yan, Kang Ping Chen, and Mian Chen. 2015a. "An asymptotic solution for fluid production from an elliptical hydraulic fracture at early-times." *Mechanics Research Communications* 63 (): 48–53. doi:10.1016/j.mechrescom.2014.12.004.

———. 2015b. "Analytical solution and mechanisms of fluid production from hydraulically fractured wells with finite fracture conductivity." *Journal of Engineering Mathematics* 92, no. 1 (): 103–122. doi:10.1007/s10665-014-9754-x.

Lu, Jing, and Djebbar Tiab. 2010. "Pseudo-Steady-State Productivity Formula for a Partially Penetrating Vertical Well in a Box-Shaped Reservoir." *Mathematical Problems in Engineering* 2010:1–35. doi:10.1155/2010/907206.

Lu, Yunhu, and Kang Ping Chen. 2016. "Productivity-Index Optimization for Hydraulically Fractured Vertical Wells in a Circular Reservoir: A Comparative Study With Analytical Solutions." *SPE Journal* 21, no. 06 (): 2208–2219. doi:10.2118/180929-PA.

Matthews, C S, F Brons, and P Hazebroek. 1954. "A Method for Determination of Average Pressure in a Bounded Reservoir." *TRANSACTIONS OF THE AMERICAN INSTITUTE OF MINING AND METALLURGICAL ENGINEERS* 201:182–191. doi:XR348. arXiv: XR348.

Prats, M, P Hazebroek, and W.R. Strickler. 1962. "Effect of Vertical Fractures on Reservoir Behavior–Compressible-Fluid Case." *Society of Petroleum Engineers Journal* 2, no. 02 (): 87–94. doi:10.2118/98-PA.

Raghavan, R. 1993. *Well Test Analysis* [in English]. Englewood Cliffs, N.J.: PTR Prentice Hall.

Ramey, H.J., and William M Cobb. 1971. "A General Pressure Buildup Theory for a Well in a Closed Drainage Area." *Journal of Petroleum Technology* 23, no. 12 (): 1493–1505. doi:10.2118/3012-PA.

Russell, D.G., and N.E. Truitt. 1964. "Transient Pressure Behavior in Vertically Fractured Reservoirs." *Journal of Petroleum Technology* 16, no. 10 (): 1159–1170. doi:10.2118/967-PA.

Sadeghi, Mohammad, Seyed Reza Shadizadeh, and Mohammad Ali Ahmadi. 2013. "Determination of Drainage Area and Shape Factor of Vertical Wells in Naturally Fracture Reservoir with Help Well testing and Developed IPR Curve." In *North Africa Technical Conference and Exhibition,* vol. 1. April 2013. Society of Petroleum Engineers. doi:10.2118/164638-MS.

APPENDIX A

RECTANGULAR LOOK-UP TABLES

Table 6. Rectangular (AR = 1) Shape Factor Look-Up Table

$I_x(\%)$	$C_{a,f}$	$I_x(\%)$	$C_{a,f}$
0.05	2.92	0.28	2.33
0.06	2.89	0.29	2.31
0.07	2.86	0.30	2.29
0.08	2.84	0.31	2.27
0.09	2.81	0.32	2.25
0.10	2.79	0.33	2.23
0.11	2.76	0.33	2.21
0.11	2.74	0.34	2.19
0.12	2.71	0.35	2.17
0.13	2.69	0.36	2.15
0.14	2.67	0.37	2.13
0.15	2.64	0.38	2.12
0.16	2.62	0.39	2.10
0.17	2.60	0.40	2.08
0.18	2.57	0.41	2.06
0.19	2.55	0.42	2.04
0.20	2.53	0.43	2.02
0.21	2.51	0.44	2.01
0.22	2.48	0.44	1.99
0.22	2.46	0.45	1.97
0.23	2.44	0.46	1.95
0.24	2.42	0.47	1.94
0.25	2.40	0.48	1.92
0.26	2.38	0.49	1.90
0.27	2.35	0.50	1.88

Table 7. Rectangular (AR = 2) Shape Factor Look-Up Table

$I_x(\%)$	$C_{a,f}$	$I_x(\%)$	$C_{a,f}$
0.05	2.92	0.28	2.33
0.06	2.89	0.29	2.31
0.07	2.86	0.30	2.29
0.08	2.84	0.31	2.27
0.09	2.81	0.32	2.25
0.10	2.79	0.33	2.23
0.11	2.76	0.33	2.21
0.11	2.74	0.34	2.19
0.12	2.71	0.35	2.17
0.13	2.69	0.36	2.15
0.14	2.67	0.37	2.13
0.15	2.64	0.38	2.12
0.16	2.62	0.39	2.10
0.17	2.60	0.40	2.08
0.18	2.57	0.41	2.06
0.19	2.55	0.42	2.04
0.20	2.53	0.43	2.02
0.21	2.51	0.44	2.01
0.22	2.48	0.44	1.99
0.22	2.46	0.45	1.97
0.23	2.44	0.46	1.95
0.24	2.42	0.47	1.94
0.25	2.40	0.48	1.92
0.26	2.38	0.49	1.90
0.27	2.35	0.50	1.88

Table 8. Rectangular (AR = 3) Shape Factor Look-Up Table

$I_x(\%)$	$C_{a,f}$	$I_x(\%)$	$C_{a,f}$
0.05	2.92	0.28	2.33
0.06	2.89	0.29	2.31
0.07	2.86	0.30	2.29
0.08	2.84	0.31	2.27
0.09	2.81	0.32	2.25
0.10	2.79	0.33	2.23
0.11	2.76	0.33	2.21
0.11	2.74	0.34	2.19
0.12	2.71	0.35	2.17
0.13	2.69	0.36	2.15
0.14	2.67	0.37	2.13
0.15	2.64	0.38	2.12
0.16	2.62	0.39	2.10
0.17	2.60	0.40	2.08
0.18	2.57	0.41	2.06
0.19	2.55	0.42	2.04
0.20	2.53	0.43	2.02
0.21	2.51	0.44	2.01
0.22	2.48	0.44	1.99
0.22	2.46	0.45	1.97
0.23	2.44	0.46	1.95
0.24	2.42	0.47	1.94
0.25	2.40	0.48	1.92
0.26	2.38	0.49	1.90
0.27	2.35	0.50	1.88

Table 9. Rectangular (AR = 4) Shape Factor Look-Up Table

$I_x(\%)$	$C_{a,f}$	$I_x(\%)$	$C_{a,f}$
0.05	2.92	0.28	2.33
0.06	2.89	0.29	2.31
0.07	2.86	0.30	2.29
0.08	2.84	0.31	2.27
0.09	2.81	0.32	2.25
0.10	2.79	0.33	2.23
0.11	2.76	0.33	2.21
0.11	2.74	0.34	2.19
0.12	2.71	0.35	2.17
0.13	2.69	0.36	2.15
0.14	2.67	0.37	2.13
0.15	2.64	0.38	2.12
0.16	2.62	0.39	2.10
0.17	2.60	0.40	2.08
0.18	2.57	0.41	2.06
0.19	2.55	0.42	2.04
0.20	2.53	0.43	2.02
0.21	2.51	0.44	2.01
0.22	2.48	0.44	1.99
0.22	2.46	0.45	1.97
0.23	2.44	0.46	1.95
0.24	2.42	0.47	1.94
0.25	2.40	0.48	1.92
0.26	2.38	0.49	1.90
0.27	2.35	0.50	1.88

APPENDIX B

RECTANGULAR SHAPE FACTOR CONFIDENCE INTERVALS

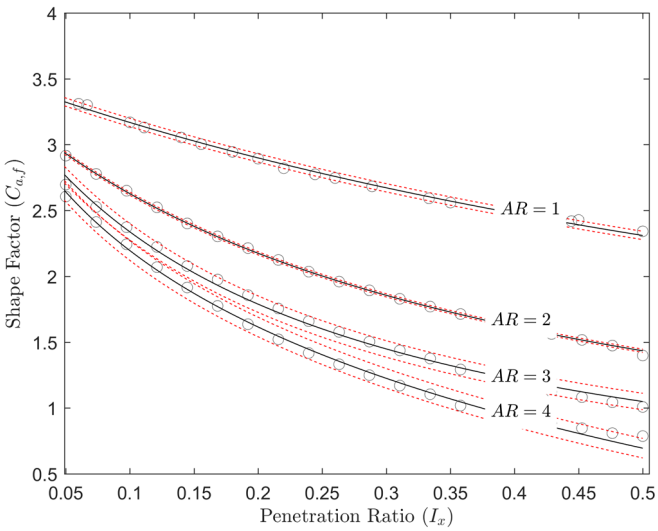

Figure 15. 95 % confidence intervals for rectangular shape factors

APPENDIX C

RHOMBOID LOOK-UP TABLE

Table 10. Rhomboid Shape Factor Look-Up Table

$I_x(\%)$	$C_{a,f}$	$I_x(\%)$	$C_{a,f}$
0.05	3.23	0.28	2.54
0.06	3.20	0.29	2.52
0.07	3.17	0.30	2.49
0.08	3.13	0.31	2.47
0.09	3.10	0.32	2.45
0.10	3.07	0.33	2.43
0.11	3.03	0.33	2.41
0.11	3.00	0.34	2.39
0.12	2.97	0.35	2.37
0.13	2.94	0.36	2.36
0.14	2.91	0.37	2.34
0.15	2.89	0.38	2.32
0.16	2.86	0.39	2.30
0.17	2.83	0.40	2.28
0.18	2.80	0.41	2.26
0.19	2.78	0.42	2.25
0.20	2.75	0.43	2.23
0.21	2.73	0.44	2.21
0.22	2.70	0.44	2.20
0.22	2.68	0.45	2.18
0.23	2.65	0.46	2.16
0.24	2.63	0.47	2.15
0.25	2.61	0.48	2.13
0.26	2.58	0.49	2.12
0.27	2.56	0.50	2.10

APPENDIX D

TRIANGULAR LOOK-UP TABLE

Table 11. Triangular Shape Factor Look-Up Table

$I_x(\%)$	$C_{a,f}$	$I_x(\%)$	$C_{a,f}$
0.05	2.92	0.28	2.33
0.06	2.89	0.29	2.31
0.07	2.86	0.30	2.29
0.08	2.84	0.31	2.27
0.09	2.81	0.32	2.25
0.10	2.79	0.33	2.23
0.11	2.76	0.33	2.21
0.11	2.74	0.34	2.19
0.12	2.71	0.35	2.17
0.13	2.69	0.36	2.15
0.14	2.67	0.37	2.13
0.15	2.64	0.38	2.12
0.16	2.62	0.39	2.10
0.17	2.60	0.40	2.08
0.18	2.57	0.41	2.06
0.19	2.55	0.42	2.04
0.20	2.53	0.43	2.02
0.21	2.51	0.44	2.01
0.22	2.48	0.44	1.99
0.22	2.46	0.45	1.97
0.23	2.44	0.46	1.95
0.24	2.42	0.47	1.94
0.25	2.40	0.48	1.92
0.26	2.38	0.49	1.90
0.27	2.35	0.50	1.88

APPENDIX E

CURVE FITTING STATISTICS

Table 12. Shape Factor Curve Fitting Statistics

Geometry	*RMSE*	R^2	Res_{Avg}	σ_A	σ_B
Rectangle (AR 1)	0.022	0.998	0.015	0.004	0.001
Rectangle (AR 2)	0.008	0.999	0.006	0.004	0.001
Rectangle (AR 3)	0.023	0.996	0.029	0.022	0.004
Rectangle (AR 4)	0.023	0.997	0.026	0.043	0.011
Rhomboid	0.007	0.999	0.010	0.003	0.001
Triangular	0.022	0.990	0.023	0.019	0.023